AIAA JOURNAL
Vol. 35, No. 9, September 1997

Simulations of High Knudsen Number Flows in a Channel–Wedge Configuration

Thuong X. Nguyen,* Choong K. Oh,† Robert S. Sinkovits‡
Naval Research Laboratory, Washington, D.C. 20375
John D. Anderson Jr.§
University of Maryland, College Park, Maryland 20742
and
Elaine S. Oran¶
Naval Research Laboratory, Washington, D.C. 20375

A rarefied hypersonic flow through a channel containing a wedge is simulated using the combined direct simulation Monte Carlo and monotonic Lagrangian grid methodologies on the massively parallel Connection Machine. Numerical issues related to the effects of resolution in terms of the simulated to actual particle ratio and the use of time averaging to obtain a statistically converged solution are discussed. Because the flow is rarefied, important aerodynamic features are diffuse compared to what is expected in a continuum flow. For example, the reattachment shock behind the trailing edge of the wedge degenerates into a diffuse viscous layer. Other low-density effects include the velocity slip, which peaks near the leading edges where the density is low, and the temperature jump of the gas adjacent to the solid surfaces, which is highest at the entrance of the channel and decreases farther downstream. The calculated skin friction and heat transfer agree well with the Reynolds analogy for boundary-layer flow.

Nomenclature

a = speed of sound
C = Chapman–Rubesin parameter
c_f = skin-friction coefficient
h = enthalpy
Kn = Knudsen number
L = length scale
M = Mach number
N = size of particle array
n = size of particle template
Pr = Prandtl number
p = pressure
q = heat flux
Re = Reynolds number
r = recovery factor
St = Stanton number
T = temperature
t = time
V = velocity
x, y = Cartesian positions or dimensions
Δ = increment
θ = wedge half-angle
λ = mean free path
μ = viscosity
ρ = density
τ = skin friction
$\bar{\chi}$ = hypersonic viscous interaction parameter

Subscripts

aw = adiabatic wall
e = edge of boundary layer
i, j = indices
max = maximum length
t = template
w = wall
0 = total
∞ = freestream

Introduction

UNDER transitional-flow conditions, the gradients of the macroscopic variables become so steep that their scale length L is on the order of the average mean free path λ. When the local Knudsen number, $Kn = \lambda/L$, is large ($Kn > 0.03$), the standard Navier–Stokes (NS) formulation cannot be used because the constitutive relations used in the continuum formulation are not valid. Thus for low-density conditions, it then becomes necessary to use a molecular approach, such as molecular dynamics,[1] a Boltzmann equation solution method,[2] or a statistical molecular method such as direct simulation Monte Carlo (DSMC).[3]

The DSMC method is an approach that has been used widely and successfully to predict the properties of transitional-regime flows. This regime is important in many aerodynamic problems and is encountered by hypersonic vehicles traveling at high altitudes. DSMC has been applied extensively to describe re-entry flows,[4,5] shock interaction on vehicles at high altitudes,[6] and chemically reacting flow.[7] The monotonic Lagrangian grid (MLG)[8] is an algorithm for optimizing particle tracking and sorting. Combining the DSMC and the MLG eliminates the fixed spatial grid of the conventional DSMC approach and results in a method that allows automatic grid refinement according to the local number density of the gas, which in turn produces higher accuracy for a given grid size.[9]

In this paper, the combined DSMC–MLG is used on the massively parallel Connection Machines (CM-5) to examine the hypersonic, transitional-regime flow through a channel with a wedge on the bottom surface. In the past, there have been related studies of hypersonic, high Knudsen number flows on ramps and cones. For example, there have been DSMC calculations of flows over a two-dimensional ramp that studied the pressure distribution along the ramp surface[10] and the shock/boundary-layer interactions as

Received Nov. 16, 1996; revision received June 2, 1997; accepted for publication June 9, 1997. This paper is declared a work of the U.S. Government and is not subject to copyright protection in the United States.

*ASEE/NRL Research Associate Fellow, Laboratory for Computational Physics and Fluid Dynamics. E-mail: tnguyen@lcp.nrl.navy.mil. Member AIAA.
†Research Engineer, Laboratory for Computational Physics and Fluid Dynamics. Member AIAA.
‡Research Physicist, Laboratory for Computational Physics and Fluid Dynamics.
§Professor, Department of Aerospace Engineering. Fellow AIAA.
¶Senior Scientist, Laboratory for Computational Physics and Fluid Dynamics. Fellow AIAA.

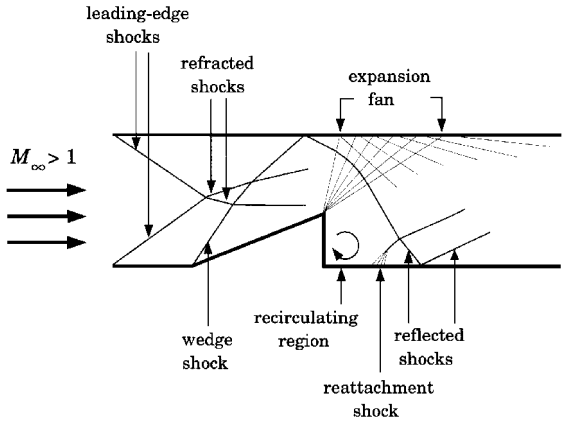

Fig. 1 Typical continuum flowfield in the channel–wedge geometry.

a function of ramp angle.[11] A study of flows over sharp cones[12] showed that the wake has minimal effects on the flow properties along the forebody of the cone, suggesting a similar behavior in the wedge case. These studies address parts of the physics in the problem to be analyzed.

Figure 1 is a sketch of the typical flow that would be expected for continuum conditions. Oblique shocks start at the leading edges of the channel and the wedge, interact with each other, and compress the flow above the slanted part of the wedge (the wedge forebody). The trailing edge of the wedge acts as a backward facing step, so that the flow expands past the step to extremely low density. The rarefied gas effects and the inaccuracies of the NS formulation may be most significant in this region. Downstream of the wedge, the flow turns parallel to the channel and forms a reattachment shock. The adverse pressure gradient across this shock causes the boundary layer to separate, and the flow reverses direction. Thus, a recirculating region is created behind the wedge. These flow features, effected by the reflected and refracted shocks, are expected to change for a rarefied flow.

From a fluid dynamic standpoint, the channel–wedge geometry produces a flowfield with many important aerodynamic features (such as shock waves, expansion fan, and boundary layers) and their complex interactions, which are not yet well understood for rarefied conditions. This study shows the effects of rarefied conditions on the flow structures by comparing the computational results qualitatively to what would be expected in a continuum flow in Fig. 1. Distributions of macroscopic properties in the flowfield are examined. The shear stress and thermal loading on the solid surfaces are calculated, and their relationship in terms of the Reynolds analogy is shown. The computed results are then compared to existing theoretical and computational data.

From an algorithmic standpoint, the problem studied here expands the application of DSMC–MLG to more complex geometry than the channel flows for which it was previously used. It is thus possible to test and develop aspects of the combined method and arrive at more specific information on the requirements for the reduction of statistical scattering. We also describe detailed resolution tests in which the grid is successively refined and the solutions are compared.

Computational Method

A detailed description of the conventional DSMC method can be found in the published literature.[3] The MLG[8] is a method for managing very large data structures. The technique ensures that the system of particles are in MLG order. That is, in this system, particles that are close in physical space are also close in array index space, and each template is made up of particles that are nearest neighbors. The MLG was combined with the DSMC resulting in a method that allows automatic grid adaptation based on the local number densities in the gas.[9]

A recent parallelization of the DSMC–MLG dramatically reduced the computational time,[13] making applications of the method to more complex flows possible. The current DSMC–MLG code optimizes the grid by using stochastic grid restructuring (SGR) to find the best grid for the problem considered.[14,15] The current code has been validated by comparing the results obtained to conventional DSMC computations by Bird for the Rayleigh problem,[4,9,13] the theoretical oblique shock angles for the low Knudsen number limit in hypersonic flows,[16] and the theoretical Mott–Smith ratio of the mean free path to the shock thickness for a monotonic gas.[16]

Computational speed and the DSMC–MLG have been extensively described in the literature. Cybyk et al.[9] showed that serial DSMC–MLG is, indeed, slower than the conventional DSMC approach in standard simplified test problems. However, there are significant advantages even in the serial form for more complex problems, such as those that require grid adaptivity to resolve high gradients or moving bodies. In the DSMC–MLG, there is, by definition, always enough particles in each cell to maintain optimal collision statistics.[9] Oh et al.[13] showed very high parallel efficiencies and speed ups of two orders of magnitude or more compared to the serial DSMC–MLG, and the efficiency increases dramatically as the number of particles increases. DSMC–MLG computations are scalable and allow simulations of millions of particles for engineering computation.

Grid Resolution and Convergence Studies

Figure 2 shows the geometry and the boundary conditions for the channel–wedge flow, and Table 1 is a summary of the flow conditions. The computational domain consists of a rectangular channel and a small freestream section upstream of the leading edges of the channel. A wedge, with half-angle θ, is placed on the bottom surface of the channel downstream from the leading edge. The channel is filled with rarefied helium gas.

The flow is initialized at Mach 5 everywhere. The wall surfaces are modeled as fully diffused boundaries. The upper and lower boundaries of the freestream section ahead of the channel are specularly reflecting. In the original applications of the DSMC–MLG, the inflow–outflow boundary condition was applied in index space. The result was that the downstream boundary could move and became distorted in physical space during the simulation.[17] However, because it is most useful to fix the length of the system a priori, a new inflow–outflow boundary condition was developed for this application.[15] In this new approach, after the particles are moved for a timestep, those particles that cross over a prescribed boundary are reintroduced at the inflow by resetting their velocities to freestream values and distributing them at random locations at the inflow boundary. As a result, the total number of simulated particles is kept constant for all times, the total molecular mass in the system is conserved, and the length of the system stays constant throughout the simulation. With this boundary condition, the inflow density is

Table 1 Flow conditions for the channel-wedge simulation

Definition	Flow condition parameter	Value
Length of channel	x_{max}	35 cm
Height of channel	y_{max}	7.5 cm
Wedge half-angle	θ	10 deg
Freestream density	ρ_{ug}	0.95×10^{-9} g/cm^3
Freestream temperature	T_∞	273 K
Freestream Mach number	M_∞	5
Wall temperature	T_w	273 K
Freestream mean free path	λ_{ug}	2.87 cm
Knudsen number	Kn	0.38
Number of particles/template	N_t	6×6

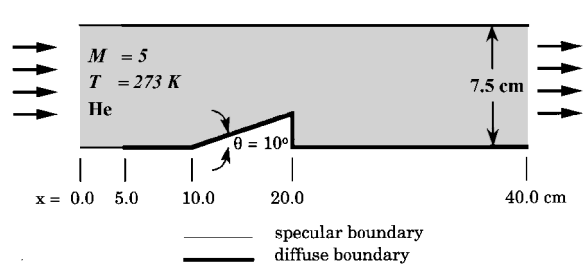

Fig. 2 Schematic of the channel–wedge flow numerical experiment.

allowed to vary during the initial transient state, but it eventually settles to a steady-state value. For our case, the inflow density settles at 0.95×10^{-9} g/cm^3, and the Knudsen number based on the channel height is 0.38, which is in the transitional flow regime.

Initial simulations showed what appeared to be a choked flow, with a normal shock standing near the inlet of the channel.[17] This phenomenon in channel flow is also a common experimental problem. Now we initialize the calculation with molecular velocities that are a slight amount (3%) above those that subsequently flow into the channel. This method is very similar to common experimental practices used to overcome choked flows that often occur in supersonic nozzles, where the initial flow velocities are slightly high and then allowed to relax to the final inflow velocity.

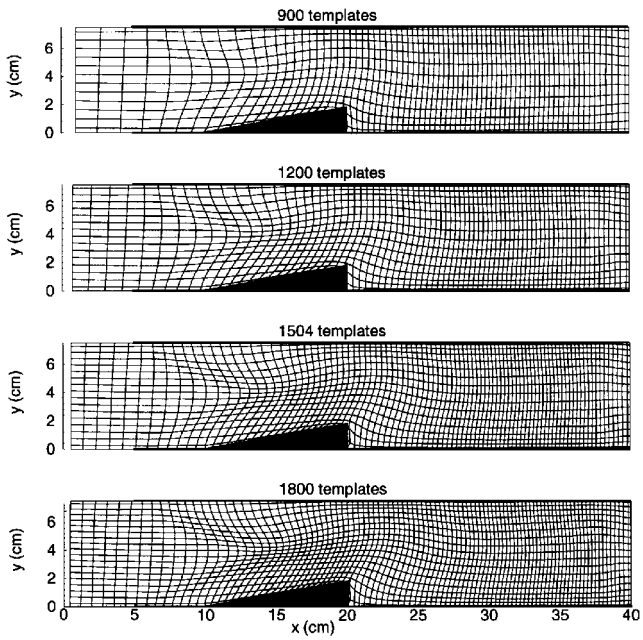

Fig. 3 MLGs for the grid resolution study.

Grid Optimization

For a given system of particles, many possible MLGs exist. The quality of these grids can vary significantly, which in turn can affect the accuracy of the solution. It is possible to find a high-quality grid for a given spatial distribution of particles by using SGR.[14] This method was implemented in the DSMC–MLG, and an intensive study was performed to obtain the optimum MLG for the channel–wedge problem.[18] The results presented in this paper are for the optimum MLG found in Ref. 18.

Grid Resolution Study

A series of simulations of the channel–wedge problem was performed to study the sensitivity of the results to the number of MLG cells. In the MLG, a cell is a template made up of nearest neighbor particles. We studied four different resolutions, with the number of templates ranging from 75×12 to 100×18 and the number of simulated particles ranging from 32,400 to 64,800. The grids for the four cases are shown in Fig. 3, and the corresponding density contours are shown in Fig. 4. The flow features obtained using the two coarsest grids are not nearly as well resolved as those using 1504 and 1800 templates, which are very similar. The two finest grids resolve all features in the flowfield. The 1504-template grid is used in the material presented subsequently. It was shown that the cell dimensions must be small compared to the scale length of the macroscopic flow gradients.[19] The averaged local Knudsen numbers for the four grid cases in Fig. 4 are 5.38, 5.74, 6.75, and 7.18, respectively. Thus, the mean free path must be at least 6.75 times that of the averaged cell dimension for accurate results. A typical calculations of 65,000 particles took about 1500 timesteps and 20 min or less to converge on the 256 node CM-5.

Steady State and Time Averaging

Because of the high ratio of actual to simulated molecules, there are large statistical fluctuations that must be reduced to obtain a meaningful solution. This is accomplished by time averaging the solution once the steady state is established. The steady state is determined when the main features are not changing, and fluctuations in scalar variables decrease. Using the 1504-template grid, the flow reaches steady state after about 1000 timesteps. The simulation was then continued for a few hundred additional timesteps before time

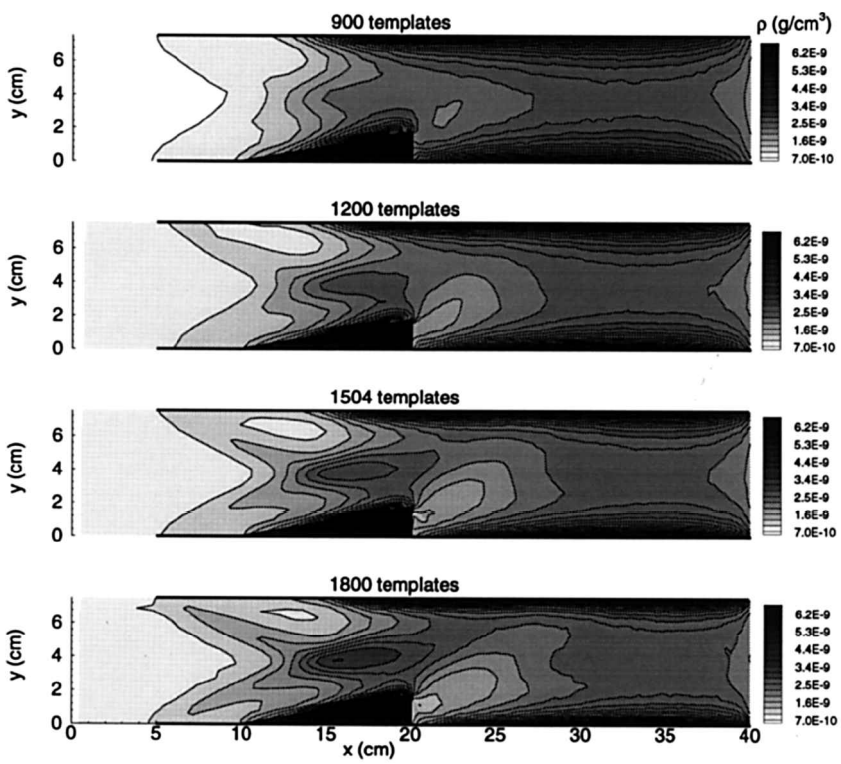

Fig. 4 Density contours for four grid resolutions; results are time averaged for 500 timesteps after steady state is reached.

averaging was started. As the number of averaged timesteps (or ensembles) increases, the statistical fluctuations decrease. The solution reached an acceptable level of statistical scattering after averaging about 500 timesteps.[18]

Analysis of the Flowfield

Flow Features and Surface Properties

Figure 5 shows the converged solution, represented by density, temperature, pressure, and Mach number contours, for the 1504-template grid with 1000-timestep averaging after steady state is reached. Even though the flow structures are diffused compared to those shown in Fig. 1, it is still possible to identify many features.

The density contours show the boundary-layer growth along the solid surfaces. The thickness of the boundary layers increases as the flow moves downstream. Near the outflow boundary, the flow expands as it leaves the channel, causing the boundary-layer thickness to decrease. The temperature contours show the temperature of the gas in the core of the channel is much higher than that near the walls, which are held at a constant temperature of 273 K. As a supersonic flow expands through a rarefaction fan, the density, temperature, and pressure of the gas decrease. This effect is seen in the region immediately downstream of the trailing edge of the wedge.

The pressure contours show two oblique shocks emanating from the upper and lower leading edges of the channel and intersecting at about 10 cm downstream of the leading edges. The oblique shock angle is $\sim$22 deg. This was estimated by measuring the angle of the pressure contours at the leading edge of the channel. The pressure contours also show that there is a third oblique shock at an angle of $\sim$40 deg emanating from the leading edge of the wedge. All of these shock structures interact near the centerline of the channel above the wedge forebody in a way similar to that shown in Fig. 1. In the upper-half of the channel, a refracted shock interacts with the boundary layer near the upper wall and reflects downstream. In the lower-half of the channel, a weaker refracted shock merges with the rarefaction region that was caused by the supersonic expansion of the flow around the sharp corner of the trailing edge of the wedge. The flow then eventually turns parallel to the wall to form a very diffuse viscous layer downstream. In a continuum flow as in Fig. 1, this layer would be a reattachment shock. The adverse pressure gradient across this reattachment region causes the boundary layer to separate, and a reverse flow is developed just behind the trailing edge of the wedge. The pressure reaches a local maximum at the bottom wall near $x = 33$ cm as the flow crosses the reattachment layer. The Mach number contours show a supersonic core flow between the subsonic boundary layers and expansion near the outflow boundary.

Figure 6 shows the density, pressure, temperature, and magnitude of velocity along the top and bottom solid surfaces of the channel. The pressure shown is the thermodynamic pressure deduced from the equation of state. Along the bottom surface, at about $x = 5$ cm, the pressure rises sharply across the leading-edge shock and increases significantly along the wedge surface due to the presence of the second oblique shock. Just ahead of the wedge trailing edge, the pressure drops across the rarefaction region as the flow expands, then increases again as the boundary layer develops. Along the top surface, the pressure increases across the leading-edge shock in the same manner as along the bottom surface. The pressure then rises markedly at about $x = 15$ cm due to the interactions between the boundary layer and the refracted shock. The temperature jump is about four times the wall temperature near the leading edge, and it decreases rapidly farther downstream. At the entrance to the channel, the slip velocity is highest. As the boundary layer develops downstream, the velocity slip decreases and drops sharply to near zero. A small increase in the slip velocity near the exit plane, $x = 40$ cm, indicates that the flow expands as it leaves the channel.

In Fig. 7, the velocity profiles at various locations along the x axis show that the boundary layers begin to form at the leading edge of the channel and grow as the flow moves downstream. There is

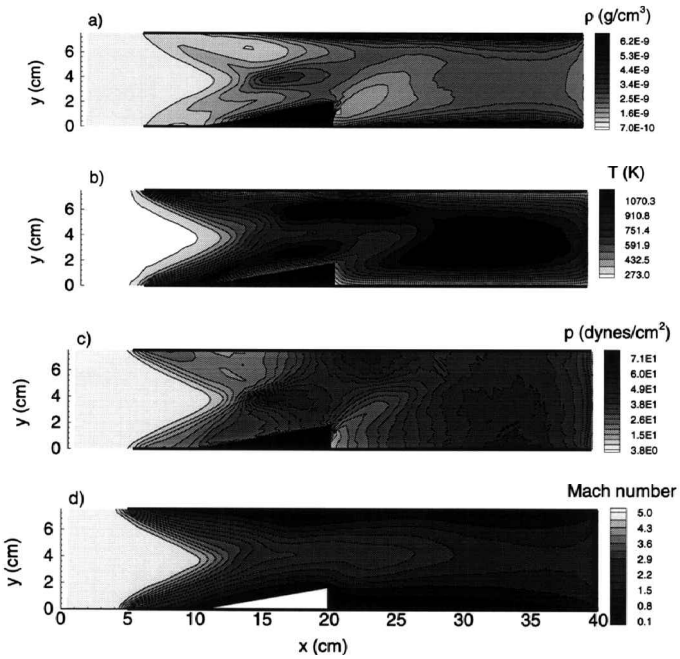

Fig. 5 Converged solution of the channel–wedge simulation; results are time averaged for 1000 timesteps after steady state is reached.

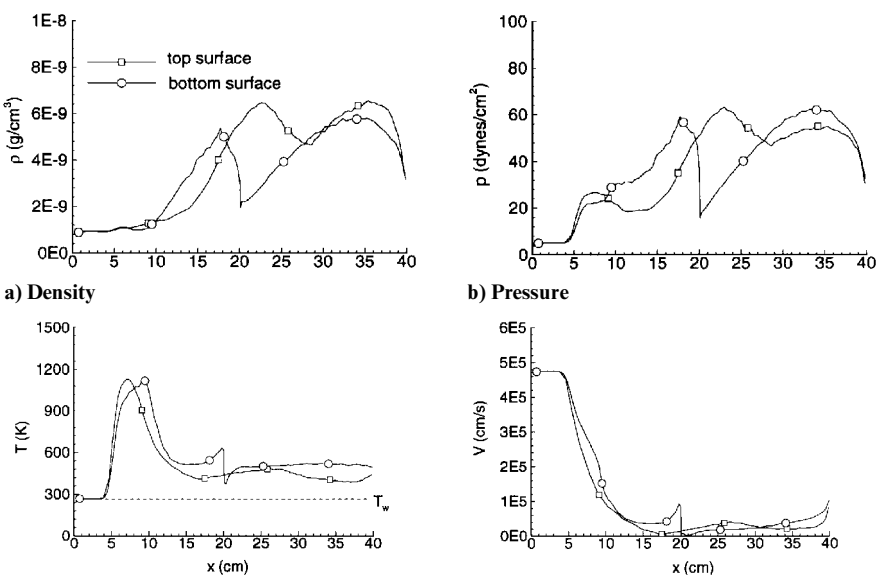

a) Density **b) Pressure**

c) Temperature **d) Magnitude of velocity**

Fig. 6 Macroscopic properties along the channel–wedge solid surfaces.

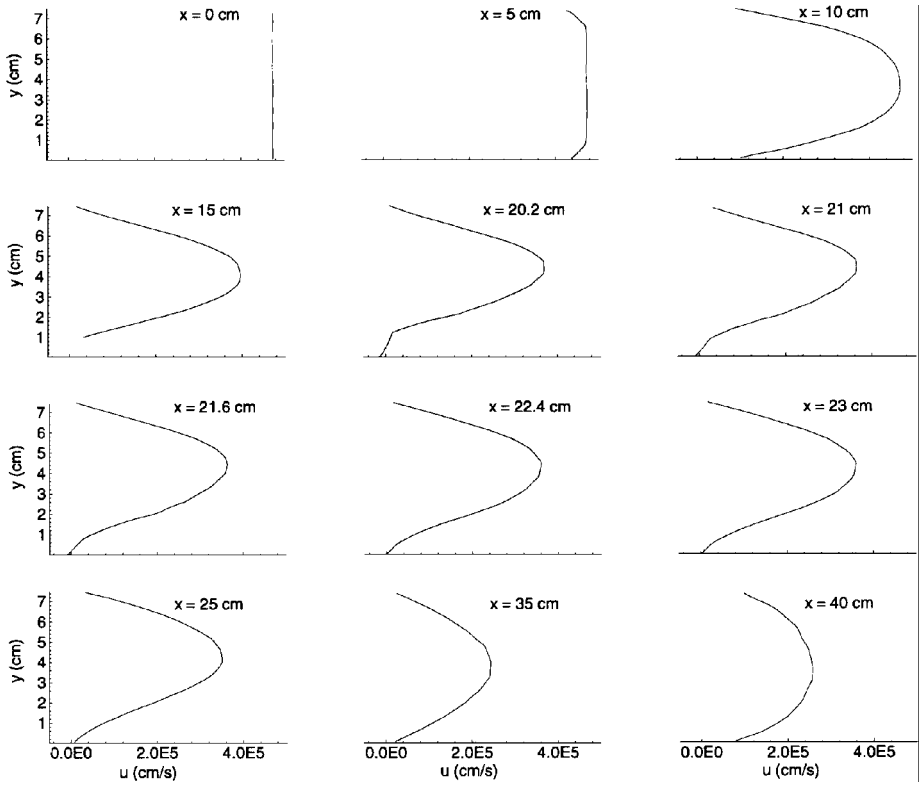

Fig. 7 Velocity profiles at various x locations along the channel.

a reverse flow (negative velocities) at the wall for 20 cm $< x <$ 22 cm.

Comparisons of Flow Properties

For an inviscid flow, with no boundary layers and infinitely thin walls, the leading-edge shocks degenerate to Mach waves. For $M_\infty = 5$ flow, the angle of such a Mach wave would be 11.54 deg. This is much smaller than the 22 deg of the shock angle calculated in this study, indicating the displacement effect of the boundary layer. The boundary layer grows rapidly in the region of the leading edge and acts as an effective body that bends the incoming streamlines upward. As a result, the shock at the leading edge is nearly normal to the surface of the channel. Across this shock at the surface, p_2/p_1 is $\sim$5, which is much smaller than the pressure rise of 29 across a continuum normal shock. This is a consequence of the low-density conditions.

Figure 8 compares the surface pressure and velocity distributions from the present study to those obtained from a DSMC calculation[11] for a near-continuum, $M_\infty = 4$ flow over a 20-deg compression corner. The surface pressure is shown as a function of the nondimensionalized distance x/L_f, where L_f is 5 cm, the length of the flat section upstream of the leading edge of the wedge. The results are in good qualitative agreement. Because of the higher freestream Mach number, the pressure in the present study is consistently higher than that of Chpoun et al.[11] The more rarefied condition ($Kn = 0.38$) in the present work resulted in a more gradual slip in the velocity adjacent to the surface. In contrast, the near-continuum condition ($Kn = 0.0047$) in Ref. 11 caused a much sharper decrease near the leading edge of the flat section. If only the flat section upstream of the leading edge of the wedge is considered, the problem reduces to that of a semi-infinite flat plate. The peak normalized pressure and skin-friction coefficient near the leading edge of the flat plate section are approximately 5.5 and 0.056, respectively. This is consistently lower than the values (7.9 and 0.085) obtained by DSMC simulations of a higher density, Mach 5 flow over a semi-infinite flat plate.[20]

Skin Friction and Heat Transfer

The skin friction τ_w on the walls of the channel is calculated by averaging the parallel momentum transfer of the molecules impinging

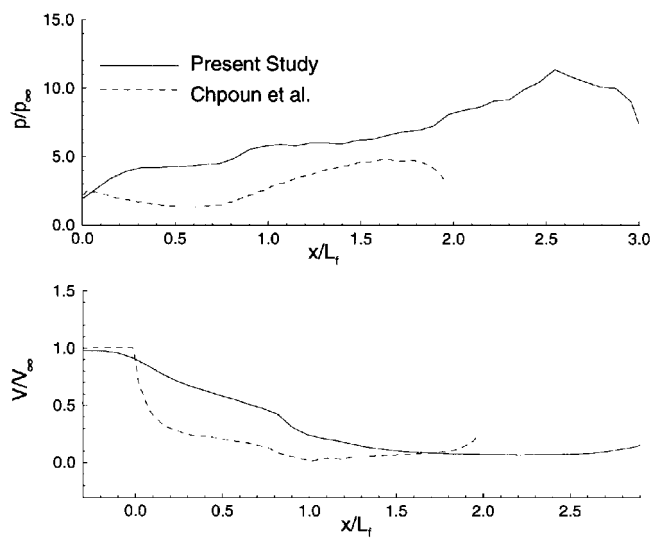

Fig. 8 Surface pressure and velocity from present study, $M = 5$ and $\theta = 10$ deg, and the simulations of Chpoun et al.,[11] $M = 4$ and $\theta = 20$ deg.

on the surfaces. The heat flux q_w at the walls may be calculated in a similar manner by replacing the parallel momentum with the energy of the impinging molecule. The results are presented in terms of the dimensionless skin-friction coefficient c_f and the Stanton number St, which are given by[21]

$$c_f = \frac{\tau_w}{\frac{1}{2}\rho_e V_e^2} \tag{1}$$

and

$$St = \frac{q_w}{\rho_e V_e (h_{\text{aw}} - h_w)} \tag{2}$$

The adiabatic wall enthalpy is evaluated in terms of the recovery factor r by[21]

$$h_{\text{aw}} = h_e + r(V_e^2/2) \tag{3}$$

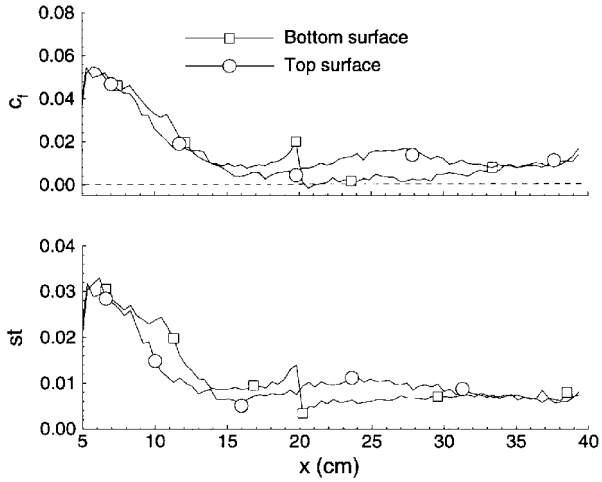

Fig. 9 Distributions of skin-friction coefficient and Stanton number along the top and bottom surface of the channel.

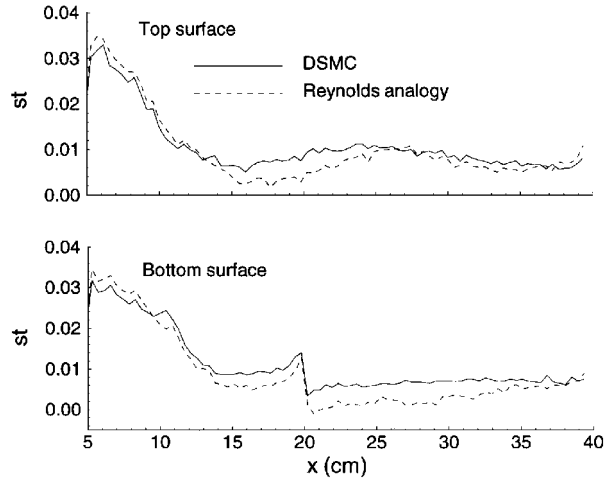

Fig. 10 Comparisons of DSMC calculated and Reynolds analogy Stanton number distributions along the top and bottom surface of the channel.

The recovery factor is taken equal to $\sqrt{Pr}$ (Ref. 21). For helium, $Pr = 0.7$ (Ref. 22). In this study, the freestream conditions are assumed at the edge of the boundary layers.

The skin friction and heat transfer to the top and bottom surfaces of the channel are shown in Fig. 9. Along the bottom surface, the value of c_f is highest near the leading edge where the high-velocity molecules are slowed down substantially by the solid boundaries. The skin-friction coefficient decreases downstream, then increases along the wedge surface, reaching a local maximum near the end of the wedge. Behind the trailing edge of the wedge, c_f becomes negative in the recirculation region. Farther downstream, c_f stays fairly constant, with a slight increase near the exit plane where the flow expands.

Along the top surface, c_f peaks near the entrance plane and decreases downstream. A local maximum of c_f occurs near $x = 25$ cm as a result of the interaction between the refracted shock and the boundary layer adjacent to the top wall. The distributions of Stanton number are similar to those of c_f. The Stanton number is positive everywhere, including the recirculating region, indicating the transfer of heat from the flow to the walls. Figure 9 represents an average of 1000 timesteps. These figures indicate that the skin friction and heat transfer require more timestep averaging than the state properties to obtain the same level of fluctuations.

The results along the top wall agree well with those obtained by a DSMC calculation of a hypersonic flow along a flat plate by Moss et al.[10] In their results, both the skin friction and heat transfer peak near the leading edge and decrease downstream. Their peak c_f is $\sim$0.07 compared to 0.056 for the top wall in this study, and their peak Stanton number is 0.02, whereas it is about 0.03 for the top wall. The quantitative differences are due to the different freestream and wall temperature conditions.

In incompressible flow theory, the Stanton number and the skin friction coefficient along a laminar flat plate are related by the Reynolds analogy[21]

$$St = c_f \tfrac{1}{2} Pr^{-\frac{2}{3}} \tag{4}$$

where Pr is the Prandtl number. Even though the flow is hypersonic in this study, it is useful to know how the results in Fig. 9 deviate from this relation, especially because it has been observed that $c_h = c_f/2$, where c_h is based on $h_0 - h_w$ for rarefied hypersonic flows over a flat plate.[20] Figure 10 compares two distributions of the Stanton number: one from the DSMC simulations (Fig. 9) and the other calculated by substituting the computed c_f into the Reynolds analogy of Eq. (4). Along the top wall, the two distributions compare very well, except for the region near the interaction between the refracted shock and the boundary layer. Along the flat section of the bottom wall upstream of the wedge, the two distributions are about the same. Downstream the curves deviate due to the presence of the wedge. These results show that the Reynolds analogy might still be applicable for high Mach number, high-Knudsen number flow along flat plates with the freestream and wall temperature conditions similar to those in this study. Other freestream and wall conditions must be investigated before the Reynolds analogy can be generalized.

Conclusion

Simulations of a rarefied, high Knudsen number flow of helium gas through a channel with a wedge have been performed using the combined DSMC–MLG algorithm. These simulations were used both to describe the flow features and their interactions under rarefied conditions and to develop and test a new approach to the DSMC algorithm. Because this work had a fluid dynamic as well as algorithmic objective, an extensive series of computations was performed for a single physical system.

The resulting computations present a highly resolved picture of a flowfield that was compared qualitatively to what would be expected in a continuum flow. Where possible, the results were compared quantitatively to theoretical analysis and computations. Because the flow is so rarefied, the flow features, such as oblique shocks, rarefaction fan, and boundary layers, and their interactions are diffuse. The pressure jump across the leading-edge shock at the surface is considerably less than that for a continuum normal shock. Downstream of the trailing edge of the wedge, the reattachment shock that is typical in a continuum flow degenerates into a very diffuse viscous layer. The effects of low-density conditions are also shown in the slip in velocity and temperature of the gas adjacent to the solid surfaces, which are highest at the entrance of the channel.

The skin-friction and heat transfer calculations show that peak shear force and thermal loading occur near the leading edges of the channel. The effects of the wedge on the flowfield are shown in local maxima of skin-friction coefficient and Stanton number distributions on the bottom wall. In addition, viscous interactions between the refracted shock and the boundary layer near the top wall result in an increase in skin friction and heat transfer. The Stanton number distribution along the top wall compare well with that calculated by the Reynolds analogy for incompressible boundary-layer flow, suggesting that the Reynolds analogy might be applicable for high-speed, rarefied flow along flat plates under conditions similar to those in this study. These results, along with the slip velocity and temperature jump data, provide a benchmark for testing phenomenological and theoretical models that attempt to extend the applicability of the NS equations to other flow regimes.

Acknowledgment

The authors acknowledge the financial support by the Post-Doctoral Fellowship from the American Society for Engineering Education, the Minta–Martin Fellowship, and the Office of Naval Research. We also wish to thank B. Z. Cybyk and J. N. Moss for their valuable help.

References

[1]Allen, M. P., and Tildesley, D. J., *Computer Simulations of Liquids*, Clarendon, Oxford, England, UK, 1990, Chap. 1.

[2]Bhatnagar, P. L., Gross, E. P., and Krook, M., "A Model for Collision Processes in Gases," *Physics Review*, Vol. 94, 1954, pp. 511–525.

[3]Bird, G. A., *Molecular Gas Dynamics and the Direct Simulation of Gas Flows*, Clarendon, Oxford, England, UK, 1994.

[4]Moss, J. N., and Bird, G. A., "Direct Simulation of Transitional Flow for Hypersonic Re-entry Conditions," AIAA Paper 84-0223, Jan. 1984.

[5]Bird, G. A., "Nonequilibrium Radiation During Reentry at 10 km/s," AIAA Paper 87-1543, June 1987.

[6]Carlson, A. B., and Wilmoth, R. G., "Shock Interference Prediction Using Direct Simulation Monte Carlo," AIAA Paper 92-0492, Jan. 1992.

[7]Dogra, V. K., Moss, J. N., Wilmoth, R. G., Taylor, J. C, and Hassan, H. A., "Effects of Chemistry on Blunt Body Wake Structure," AIAA Paper 94-0352, Jan. 1994.

[8]Boris, J. P., "A Vectorized Near-Neighbors Algorithm of Order *N* Using a Monotonic Logical Grid," *Journal of Computational Physics*, Vol. 66, No. 1, 1986, pp.1–20.

[9]Cybyk, B. Z., Oran, E. S., Boris, J. P., and Anderson, J. D., "Combining the Monotonic Lagrangian Grid with a Direct Simulation Monte Carlo Model," *Journal of Computational Physics*, Vol. 122, No. 2, 1995, pp. 323–334.

[10]Moss, J. N., Price, J. M., and Chun, C., "Hypersonic Rarefied Flow About a Compression Corner—DSMC Simulation and Experiment," AIAA Paper 91-1313, June 1991.

[11]Chpoun, A., Lengrand, J. C., Cohen, L., and Heffner, K. S., "DSMC Numerical Investigation of Rarefied Compression Corner Flow," AIAA Paper 93-3096, June 1993.

[12]Taylor, J. C., Moss, J. N., and Hassan, H. A., "Study of Hypersonic Flow Past Sharp Cones," AIAA Paper 89-1713, June 1989.

[13]Oh, C. K., Sinkovits, R. S., Cybyk, B. Z., Oran, E. S., and Boris, J. P., "Parallelization of DSMC Combined with the Monotonic Lagrangian Grid," *AIAA Journal*, Vol. 34, No. 7, 1996, pp. 1363–1370.

[14]Sinkovits, R. S., Boris, J. P., and Oran, E. S., "A Technique for Regularizing the Structure of a Monotonic Lagrangian Grid," *Journal of Computational Physics*, Vol. 108, No. 2, 1993, pp. 368–372.

[15]Nguyen, T. X., "Enhancements of the Parallelized DSMC–MLG Method for Applications to Complex Hypersonic Transitional-Regime Flows," Ph.D. Dissertation, Aerospace Engineering, Univ. of Maryland, College Park, MD, May 1995.

[16]Oh, C. K., Oran, E. S., and Sinkovits, R. S., "Computations of High-Speed, High-Knudsen-Number Microchannel Flows," *Journal of Thermal Physics and Heat Transfer* (to be published).

[17]Cybyk, B. Z., "Combining the Monotonic Lagrangian Grid with Direct Simulation Monte Carlo; a New Approach for Low-Density Flows," Ph.D. Dissertation, Aerospace Engineering, Univ. of Maryland, College Park, MD, May 1994.

[18]Nguyen, T., Oh, C., Sinkovits, R., Anderson, J., and Oran, E., "Simulations of Hypersonic Rarefied Gas Flows Using DSMC–MLG," Naval Research Lab. Rept. NRL/MR/6404-97-7917, Washington, DC, 1997.

[19]Bird, G. A., "Perception of Numerical Methods in Rarefied Gas Dynamics," *Rarefied Gas Dynamics: Theoretical and Computational Techniques*, edited by E. P. Muntz, Vol. 118, Progress in Astronautics and Aeronautics, AIAA, Washington, DC, 1989.

[20]Elizarova, T. G., Graur, I. A., Lengrand, J. C., and Chpoun, A., "Rarefied Gas Flow Simulation Based on Quasigasdynamic Equations," *AIAA Journal*, Vol. 33, No. 12, 1995, pp. 2316–2324.

[21]Anderson, J. D., Jr., *Hypersonic and High Temperature Gas Dynamics*, McGraw–Hill, New York, 1989, pp. 236, 249, and 256.

[22]White, F. M., *Viscous Fluid Flow*, McGraw–Hill, New York, 1974, p. 80.

W. Oberkampf
Associate Editor